PCCP

PAPER

View Article Online
View Journal | View Issue

Cite this: *Phys. Chem. Chem. Phys.*, 2016, **18**, 1191

Structural motifs of 2-(2-fluoro-phenyl)-ethylamine conformers†

Nitzan Mayorkas,[a] Hanan Sachs,[a] Markus Schütz,[b] Shun-ichi Ishiuchi,[c] Masaaki Fujii,[c] Otto Dopfer[b] and Ilana Bar*[a]

Received 11th October 2015,
Accepted 19th November 2015

DOI: 10.1039/c5cp06131h

www.rsc.org/pccp

Vibronic and vibrational spectra of 2-(2-fluoro-phenyl)-ethylamine (2-FPEA) conformers were measured in a molecular beam by resonant two-photon ionization (R2PI), ultraviolet–ultraviolet hole burning (UV–UV HB) spectroscopy, and ionization-loss stimulated Raman spectroscopy (ILSRS). The measured ILSR spectral signatures in the survey spectra of the amino group region and in the broad spectral range revealed the presence of five different conformers, which were confirmed by the HB spectra. The determination of the structures of the conformers of 2-FPEA was assisted by quantum chemical calculations of the torsional potential energy surface and of the scaled harmonic Raman spectra. Comparison of the measured ILSR spectra with the calculated Raman spectra allowed us to identify one *gauche* structure with the ethylamino side chain folded toward the fluorine atom, two *gauche* structures with the ethylamino side chain folded to the opposite side and two *anti* conformers with extended tails. The effect of fluorination on the spectra and on the stability and structures of these species is discussed.

1. Introduction

The presence of various degrees of freedom in flexible molecules may lead to ridged potential energy surfaces (PESs) with several conformational minima. Nevertheless, even if a particular molecule can possess multiple conformational structures, only one or a few favored structures may be observed, depending on the relative energies of their minima, the barrier heights which separate them and the possible paths for isomerization. By finding the preferential conformations, it is plausible to obtain information on intramolecular forces in isolated molecules and even on the delicate balance between the intra- and intermolecular forces for a specific molecule and for those situated in its vicinity, respectively.[1–4] This is of particular importance for molecules and their clusters with biological activity, which play a significant role in biospecific recognition at a receptor site, *via* hydrogen bonds or London dispersion forces. Yet, finding the spatial arrangements of isolated biomolecules is only a very preliminary step toward assessment of their function in actual biological environments.

One class of compounds that has gained considerable interest during recent years is that of neurotransmitters (NTs), which contain a rigid skeleton and an ethylamino side chain. NTs are endogenous messenger compounds, responsible for transmission, enhancement and modulation of neural signals across the synapse between neurons. The transmission process occurs through hydrogen bonding of the NT to a receptor protein with specific amino acid residues in a "key and lock" recognition process.[5] Since NTs are flexible molecules, they can modify their conformation easily, but their binding sites must be situated at specific positions. Therefore, the conformation of the flexible key, which is recognized by the usually more rigid lock, must be quite limited to achieve high selectivity.[6]

Indeed, the conformational topography of representative NTs appearing in the gas phase as neutral,[7–20] fluorinated,[21,22] protonated[23,24] and cluster[10,25,26] species was explored by various spectroscopic methods, assisted by quantum chemical calculations. In these studies, comparison of the measured spectral signatures with the calculated spectra enabled one to find the corresponding structures and to unravel their intrinsic properties at the most fundamental level.

For example, 2-phenylethylamine (PEA), among the simplest aromatic biogenic amines and the building block for various NTs and neurologically active molecules, was found to fold into four different conformers, while rotating about the C–C and C–N single bonds in the ethylamino side chain.[7,9b,10,11,16,18a] The two lowest and two highest energy conformers of PEA favored structures with folded (*gauche*) and extended (*anti*) tails, where in the former, one of the amino hydrogen atoms

[a] *Department of Physics, Ben-Gurion University of the Negev, Beer-Sheva 84105, Israel. E-mail: ibar@bgu.ac.il*
[b] *Institut für Optik und Atomare Physik, Technische Universität Berlin, Hardenbergstr. 36, 10623 Berlin, Germany*
[c] *Chemical Resources Laboratory, Tokyo Institute of Technology, Yokohama 226-8503, Japan*

† Electronic supplementary information (ESI) available. See DOI: 10.1039/c5cp06131h

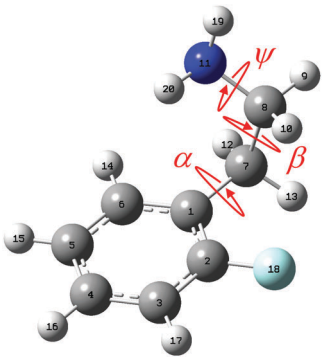

Fig. 1 The 2-(2-fluoro-phenyl)-ethylamine molecule and its dihedral angles, which determine the possible conformations.

was oriented towards the aromatic ring, forming weak N–H$\cdots\pi$ hydrogen bonds.

Recalling that the activity of NTs and drugs can be altered by fluorine substitution,[27–30] and that structural information on these compounds is only scantily available, it is anticipated that the substitution of a single hydrogen atom, in different positions of the phenyl ring of PEA, might provide a venue for testing the effect of fluorination on the conformational landscape.

In the present work, we extended our studies from PEA to 2-(2-fluoro-phenyl)-ethylamine (F–C_6H_4–CH_2–CH_2–NH_2, 2-FPEA), Fig. 1, an asymmetric structure obtained by fluorine substitution at the *ortho* position. The presence of fluorine at this position, nearby the ethylamino chain, is expected to be the most effective in inducing some conformational variations and hence revealing the structural motifs in 2-FPEA is of much interest. Indeed, the conformational landscape of 2-FPEA has been characterized recently by rotational Fourier-transform microwave spectroscopy in a molecular beam, and five conformers were identified with the help of *ab initio* calculations.[22] In the present work, one-color mass-selected resonant two-photon ionization (R2PI), ultraviolet–ultraviolet hole burning (UV–UV HB), and ionization-loss stimulated Raman spectroscopy (ILSRS),[18,31] namely stimulated Raman-ultraviolet (SR-UV) hole-burning spectroscopy, were employed to determine the characteristic vibrational and vibronic spectral signatures. The ILSRS signatures were obtained by measuring the depletion of the various ground state species, through SR excitation and R2PI probing, first in the NH stretch region and then in the broad spectral range between 400–1700 and 2750–3500 cm^{-1}. The survey spectra in the amino group region and those in the broad range were measured while fixing the UV laser on each of the dominant features of the R2PI spectrum and on features related to the transitions to the origins, respectively. The ILSR spectral signatures were compared to calculated Raman spectra, obtained by quantum chemical calculations, allowing identification of the involved structures. Similar to the microwave study,[22] the existence of five monomer structures, three *gauche* (one with the ethylamino tail folded toward the fluorine atom, and two to the opposite side) and two *anti* conformers, with extended tails was revealed. The calculated torsional PES confirmed that these are the most stable structures of the 2-FPEA conformers, being separated by high potential energy barriers.

2. Methods

a. Experimental techniques

The one-color R2PI and ILSR experiments in Beer-Sheva were performed similarly to previous studies,[18,26] while using a pumped Wiley–McLaren home-built time-of-flight mass spectrometer (TOFMS).[32] Briefly, the TOFMS included a differentially pumped source and a main detection chamber, separated by a skimmer with a 2.0 mm diameter (dia.) aperture. A stream of carrier gas (Ar), at a pressure of about 1 bar, was directed through the vapor of a 2-FPEA sample, purchased from Sigma-Aldrich (99% pure), held in a small reservoir at room temperature. The prepared gas mixture was then expanded through a solenoid-based pulsed valve (0.8 mm dia. orifice) operating at 10 Hz and then passed through the skimmer before entering into the main vacuum chamber. The generated molecular beam was introduced into the main chamber, while pointing toward the detection plane.

In the interaction region of the TOFMS, the molecular beam was crossed by the laser beams, allowing measurement of mass-selected R2PI and ILSR spectra. The R2PI spectrum was measured using a tunable frequency-doubled pulsed neodymium: yttrium aluminum–garnet (Nd:YAG)-pumped dye laser (UV) ($\sim$5 ns pulses, 10 Hz frequency and energy of $<$10 μJ). The ILSR spectra were measured while employing an additional Nd:YAG laser system that provided the beams for SR scattering, and parking the UV laser on resonances, related to the different conformers. This laser provided the second harmonic (532 nm) ($\sim$5 ns pulses at 10 Hz), which was split in a one to four ratio, so that the former served as the pump beam, ω_p, and the latter pumped a dye laser to generate a tunable Stokes beam, ω_S. The counterpropagating vertically polarized ω_p and ω_S beams with energies of $\sim$17 and 25 mJ per pulse, respectively, were focused with 35 and 30 cm focal length (f.l.) planoconvex lenses and aligned to spatially and temporally overlap in the interaction region of the TOFMS. These beams also overlapped the UV beam, focused by the 35 cm f.l. lens, but preceded it by $\sim$30 ns.

Ions obtained by the different methods were detected by a microchannel plate and fed into a home-made fast preamplifier, allowing measurement of the mass spectra, or the integrated intensity of the molecular ion peak with a fast digital oscilloscope. The R2PI and ILSR spectra were obtained by measuring the integrated ion signal as a function of the UV and ω_S beam wavelengths, respectively. For each conformer, three to ten ILSR spectra were measured and averaged for obtaining suitable signal-to-noise levels.

The experimental setup in Tokyo to measure the one-color R2PI and UV–UV HB spectra is described in detail elsewhere.[33] Briefly, it couples a supersonic expansion with a linear TOFMS. 2-FPEA vapor (Sigma-Aldrich, 99%) seeded in 2 bar Ar carrier gas was supersonically expanded through a pulsed valve. To measure R2PI spectra a tunable UV laser (several μJ) was focused on the molecular beam in the ionization region of the linear TOFMS. To measure the UV–UV HB spectra, one UV laser (probe, several μJ) was set to the $S_1 \leftarrow S_0$ band origin of a specific conformer and a second tunable UV laser (sub mJ) was fired 1 μs before to induce the isomer-specific depopulation,

resulting in dips in the R2PI spectra. Both UV lasers were generated by frequency doubling of Nd:YAG pumped dye lasers. The pulsed valve and the second UV laser (probe) were operated at 20 Hz, while the first UV laser (burn) was operated at 10 Hz to obtain R2PI signals with and without burn lasers. The signals of alternating triggers were divided to derive a normalized HB spectrum, corrected for source fluctuations.

b. Calculations

Initial geometry optimizations of the 2-FPEA conformers were performed by the MMFF94s force field in Avogadro.[34] These initial geometries were then introduced in the GAUSSIAN 09 package[35] to carry out density functional theory (DFT) calculations for determining the geometric, energetic and vibrational characteristics of the 2-FPEA conformers. The geometric optimization was carried out using ''tight'' self-consistent field convergence criteria and ''ultrafine'' integration grids. The optimizations were performed by the Becke three parameter hybrid functional combined with the Lee–Yang–Parr correlation functional (B3LYP)[36,37] and by dispersion-corrected DFT, using the M06-2X functional.[38] The 6-311++G(d,p) basis set was used for both methods. The optimized structures were then used for *ab initio* single point energy calculations, with the second order Møller–Plesset perturbation theory (MP2)[39] and the same basis set, to confirm the energetic ordering.

The optimized geometries were also used for calculation of the harmonic vibrational frequencies and the Raman activities at the same DFT levels of theory. The location of these geometries at true local minima on the PES was confirmed by the positive values of all calculated vibrational frequencies. Since the harmonic frequencies derived from the B3LYP and M06-2X functionals overestimate the fundamental frequencies measured in the experiment, the harmonic frequencies were scaled by the factors 0.956, 0.964 and 0.964 and 0.943 for the former and by 0.946, 0.953 and 0.949 and 0.974 for the latter functional. The first three factors for each functional were used for scaling the N–H stretches, C–H stretches of the ring and C–H stretches of the ethylamino group and the last ones for the low (<1700 cm^{-1}) frequency ranges, respectively. These factors were determined by comparing the calculated and measured spectra of conformer G2h (see below) and used for all other conformers. In addition, the Raman activities were converted to Raman intensities, according to the procedure of ref. 18*d*.

Essentially, the flexible ethylamino side chain has four coordinates with large-amplitude motion, namely internal rotation about the C8–N, C7–C8, and C1–C7 bonds, *i.e.*, the ψ, β, and α dihedral angles (Fig. 1), respectively, and inversion of the NH_2 group.[12*c*] Nevertheless, the nine lowest-energy conformers of 2-FPEA (see below), obtained by the calculations, have almost similar configurations about the C1–C7 bond (the angle α deviates by $<8^\circ$ from 90°). In addition, the inversion of the NH_2 group has a high barrier. Therefore, since the lowest energy conformers of 2-FPEA mainly differ in the ψ and β dihedral angles, it was possible to calculate the three dimensional (3D) torsional PES of 2-FPEA, using the MP2/6-311++G(d,p) level of theory, while considering internal rotation about these angles.

3. Results and discussion

a. Resonant two-photon ionization and survey ionization-loss stimulated Raman spectra

The mass-selected one-color R2PI spectrum of 2-FPEA, in the $S_1 \leftarrow S_0$ band origin region, is shown in Fig. 2(a). The R2PI spectrum is dominated by an intense origin at 37 608 cm^{-1} and some other features shifted to the blue and red side, respectively. Since this R2PI spectrum was monitored by measuring the ion signal appearing in the same mass channel (m/z 139), it is anticipated that it includes features related to all different conformers of 2-FPEA present in the beam, where some of them correspond to transitions to the origins, *i.e.*, 0_0^0 vibronic states, or to excited vibronic states of the various conformers. Usually these bands are distinguished by UV–UV or IR–UV HB spectroscopy,[3,10,12] which can identify the vibronic transitions to the 0_0^0 or higher states, related to each of the species in the R2PI spectrum. However, in previous studies,[18] we noticed that the very sharp ILSRS peaks, reflecting the Q-branches of the vibrational transitions, enable determination of very small shifts in their position. Therefore, we decided to test the possibility to use ILSR spectroscopy for discerning between the vibronic transitions related to the S_1 origins or excited states of the different conformers.

These survey spectra were measured while using the SR beams for vibrational excitation and tuning the ω_S beam through the limited spectral range of the amino stretches, when the time-delayed UV laser was parked on each of the observed R2PI transitions. When the frequency differences of the SR laser beams, ω_P–ω_S, matched the amino group vibrational frequencies, depletion of the population of the vibrational ground state of 2-FPEA molecules occurred, reducing the number of produced ions, and thus generating the corresponding ILSR spectra.

The ILSR survey spectra, shown in Fig. 3(a)–(n), probed the 3300–3450 cm^{-1} range, including the symmetric and antisymmetric N–H stretches of the 2-FPEA conformers, while parking on the peaks of the bands carrying significant intensity and appearing in the R2PI spectrum of Fig. 2(a). It can be noticed that the spectra in the various panels show similar or different Raman shifts for the N–H stretches, represented by identical or other colors, respectively. Actually, the small variations in the shifts of symmetric and antisymmetric N–H stretches of 3346 and 3414 [panels (a), (b), (c), (d), (e) and (g)], 3349 and 3416 [panel (f)], 3345 and 3408 [panels (h) and (k)], 3347 and 3408 [panels (i), (m) and (n)], and 3350 and 3413 cm^{-1} [panels (j) and (l)], respectively, were considered to indicate conformer-specificity. In most cases both frequencies differ, but the spectra of Fig. 3(h) and (k) as well as Fig. 3(i), (m) and (n) show a similar position for the antisymmetric N–H stretch (3408 cm^{-1}). Yet, the different frequencies of the symmetric N–H stretches and in most cases of both symmetric and antisymmetric N–H stretches, respectively, allowed sorting the spectra into five different types, plotted with black, cyan, blue, magenta and green colors, respectively. Following the assignment of the structures of the observed conformers, from the ILSR spectra (see below), the colors were found to correspond to G1h,

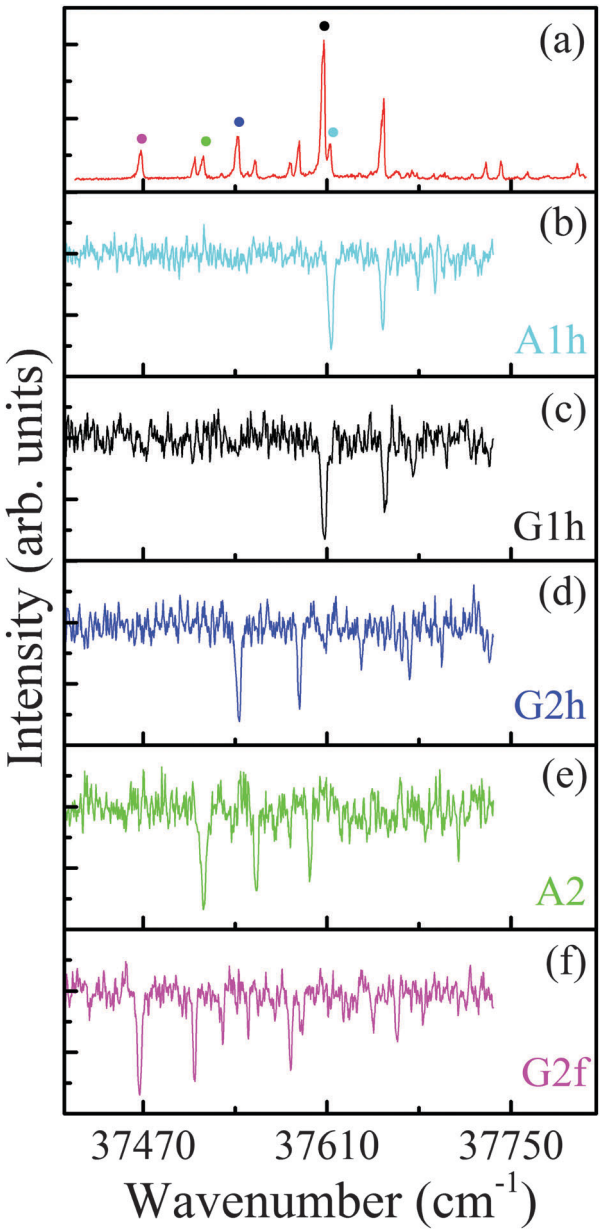

Fig. 2 (a) One-color resonantly enhanced two photon ionization spectrum of the $S_1 \leftarrow S_0$ electronic transitions of the 2-(2-fluoro-phenyl)-ethylamine monomer measured in the mass channel *m/z* 139 under water-free conditions. The bands labeled with colored circles correspond to the 0_0^0 electronic origins of the conformers A1h, G1h, G2h, A2 and G2f. (b–f) Two-color ultraviolet–ultraviolet hole burning spectra recorded with the probe laser set resonant to the S_1 origin of the five conformers.

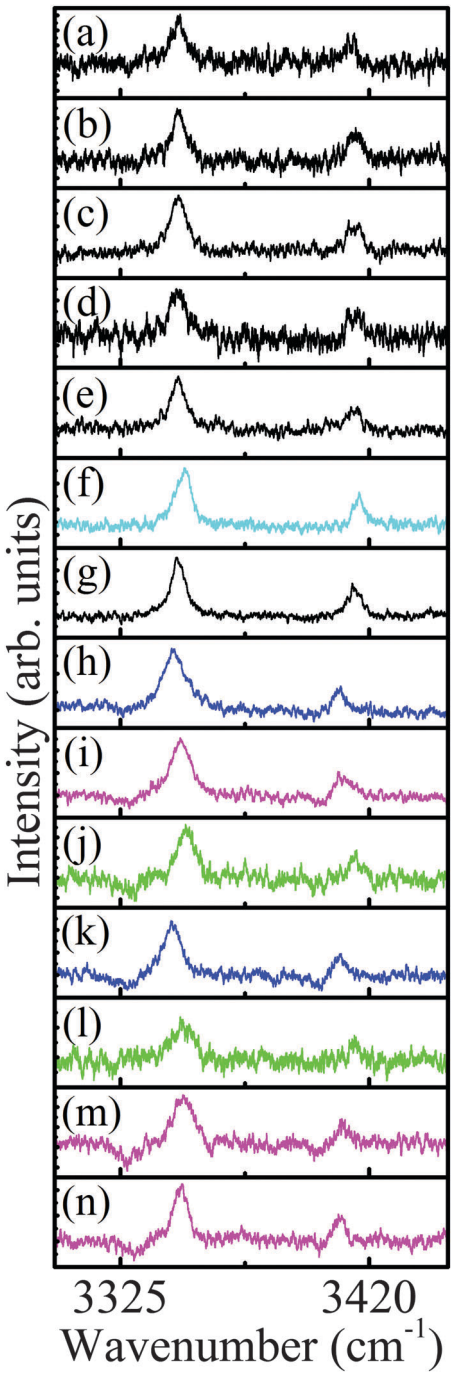

Fig. 3 Survey ionization-loss stimulated Raman spectra of the conformers of 2-(2-fluoro-phenyl)-ethylamine in the N–H stretch region, displayed in panels (a) to (n). The spectra corresponding to conformers G1h, A1h, G2h, G2f, and A2 are represented by black, cyan, blue, magenta and green, respectively. The probe laser was parked on the bands appearing at 37800, 37763, 37742, 37731, 37654, 37613, 37608, 37589, 37582, 37556, 37543, 37516, 37509 and 37468 cm^{-1} for panels (a) to (n), respectively.

A1h, G2h, G2f, and A2 conformers of 2-FPEA, respectively. This notation of the conformers is according to that used by Melandri *et al.*,[22] who also detected the same five conformers in the molecular beam by using rotational spectroscopy.

Our above classification allowed distinguishing between the R2PI features of 2-FPEA [Fig. 2(a)], where some were associated to the origins of the different conformers and others to excited vibronic states, where the former were marked by the corresponding colored circles. For most conformers, the first excited vibronic states at ≈ 40 cm^{-1} are observed, while for G1h additional states at higher frequencies could also be observed. This is reasonable, considering that the G1h exhibits the most intense feature for the 0_0^0 vibronic state and appears to be the most populated one in the molecular beam. It is worth noting

that the R2PI spectrum of 2-FPEA is richer than that of PEA, which showed only four dominant features, corresponding to the four different conformers.[10,18a] This is reasonable, considering the relative energies of the conformers of the two compounds (see below) and probably the more intense transition moments in 2-FPEA.

b. UV–UV hole burning spectra

The R2PI spectrum of 2-FPEA measured from 37 380 to 37 750 cm^{-1} in Tokyo was similar in appearance to the one measured in Beer-Sheva [Fig. 2(a)] and is therefore not shown here. UV–UV HB spectra measured to distinguish the electronic transitions of the various 2-FPEA conformers are shown in Fig. 2(b)–(f). The probe laser was set to the $S_1 \leftarrow S_0$ transitions marked with the circles in the R2PI spectrum. The HB spectra together with the R2PI spectrum revealed five different conformers, which are in full agreement with those derived from the R2PI/ILSR spectra in Fig. 3–5. The latter provide the conformational assignment as shown in Fig. 2 and listed in Table 1. Next to the band origins all other transitions in the R2PI spectrum appear in the HB spectra except peaks above 37 715 cm^{-1} due to insufficient laser power.

c. Ionization-loss and -gain stimulated Raman spectra

Conformer-specificity in 2-FPEA was confirmed by measurement of the ILSR spectra of the different species in a broad spectral range. In particular, the upper traces of Fig. 4(a)–(e) and 5(a)–(e) show the low (400–1700 cm^{-1}) and high (2750–3500 cm^{-1}) frequency ranges of the ILSR spectra (see data in

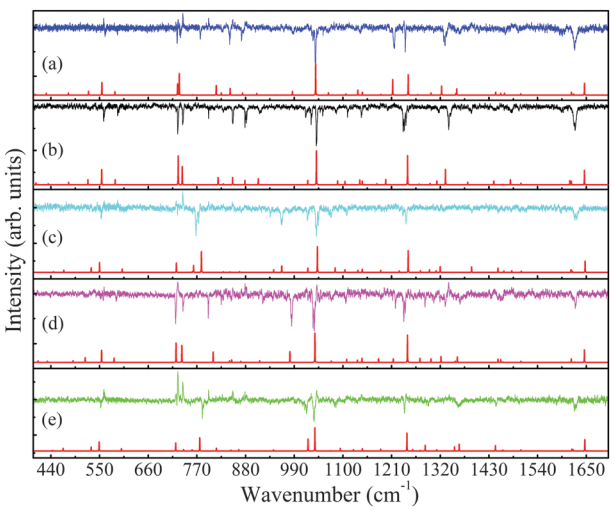

Fig. 4 Ionization-loss stimulated Raman spectra of the five conformers of 2-(2-fluoro-phenyl)-ethylamine, G2h (a), G1h (b), A1h (c), G2f (d) and A2 (e) (their geometries appear in Fig. 6), in the 400–1700 cm^{-1} energy range. Below each measured spectrum a calculated one, exhibiting the closest agreement, is shown. The computed spectra are based on scaled harmonic vibrational frequencies and on Raman intensities, obtained according to ref. 18*d*. The frequencies and Raman activities (used for derivation of the intensities) of the different conformers were calculated at the M06-2X/6-311++G(d,p) level and convoluted with Lorentzian lines of full width at half maximum of 0.5 cm^{-1}.

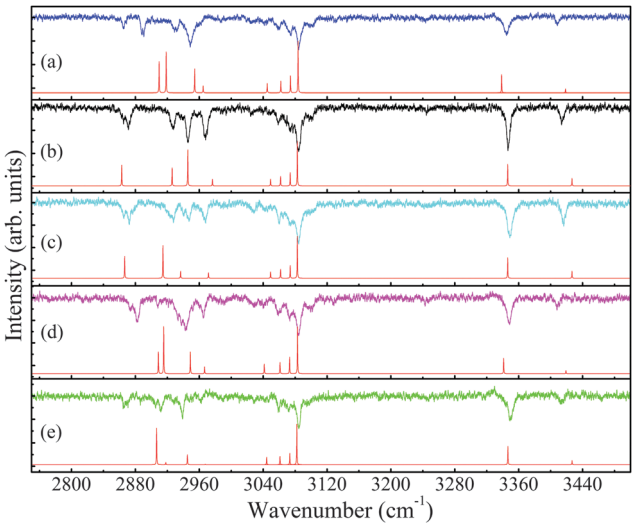

Fig. 5 Ionization-loss stimulated Raman spectra of the five conformers of 2-(2-fluoro-phenyl)-ethylamine, G2h (a), G1h (b), A1h (c), G2f (d) and A2 (e) (their geometries appear in Fig. 6), in the 2750–3500 cm^{-1} energy range. Below each measured spectrum a calculated one, exhibiting the closest agreement, is shown. The computed spectra are based on scaled harmonic vibrational frequencies and on Raman intensities, obtained according to ref. 18*d*. The frequencies and Raman activities (used for derivation of the intensities) of the different conformers were calculated at the M06-2X/6-311++G(d,p) level and convoluted with Lorentzian lines of full width at half maximum of 0.5 cm^{-1}.

Table 1 Vibronic transition frequencies (cm^{-1}) of the conformers of 2-(2-fluoro-phenyl)-ethylamine, obtained from the one-color resonant two-photon ionization and from the two-color ultraviolet–ultraviolet hole burning spectra, and their assignment

R2PI (cm^{-1})	Conformer assignment	UV–UV HB (cm^{-1})				
		G2f	A2	G2h	G1h	A1h
37 468	G2f $S_1 \leftarrow S_0$	37 468				
37 509	G2f	37 509				
37 516	A2 $S_1 \leftarrow S_0$		37 516			
37 531	G2f	37 531				
37 543	G2h $S_1 \leftarrow S_0$			37 543		
37 550	G2f	37 550				
37 556	A2		37 556			
37 569						
37 582	G2f, A2	37 582	37 582			
37 589	G2h			37 589		
		37 591				
37 597	A2		37 597			
37 608	G1h $S_1 \leftarrow S_0$, G2h			37 609	37 608	
37 613	A1h $S_1 \leftarrow S_0$					37 613
				37 636		
		37 645				
37 654	G1h, A1h				37 654	37 653
37 663	G2f	37 664				
37 671	G2h			37 673		
37 675	G1h				37 676	
37 679	A1h					37 679
37 691	A1h					37 692
				37 697		
37 700	G1h				37 701	
			37 710			
37 720						
37 731	G1h					
37 742						
37 763	G1h					
37 800	G1h					

Table S1 of the ESI†), and were measured by parking the UV laser on the 0_0^0 vibronic states marked in Fig. 2 as colored circles and corresponding to A1h, G1h, G2h, A2 and G2f, respectively. It can be clearly seen that each spectrum includes peaks pointing down, reflecting the *Q*-branches of the transitions to different vibrational modes. The observed features show different positions, not only for the N–H stretches, but also for other bands, leading to different patterns with characteristic vibrational signatures for each of the five conformers of 2-FPEA.

Furthermore, in the low frequency range, Fig. 4, some of the ILSR spectra, presented in panels (a), (c), (d) and (e) and corresponding to conformers G2h, A1h, G2f and A2 of 2-FPEA, respectively, include in addition to the loss lines (pointing down) also some gain lines (pointing up). These lines are a result of SR-induced gains, due to ionization probing of the upper Raman-pumped levels.[18c,d,40] In this process, the amount of photoionized 2-FPEA molecules increases, as a result of resonant R2PI probing of excited SR transitions. This leads to enhanced mass selected ion signals as a function of the ω_S frequency and consequently to observation of some Raman resonances by gain lines.

Examination of the Raman shifts, exhibited by the gain features in the different spectra, shows that they exactly match the position of the loss lines of conformer G1h (the most populated one, as suggested by its intensity in the R2PI spectrum, Fig. 2(a)). Some of the lines appear in all spectra, although they are excited by different UV wavelengths (depending on the UV excitation wavelength for each conformer), while others only at a specific UV wavelength. In some cases, when the gain- and loss-lines are very nearby, the appearance of the former lines in the spectra perturbs the latter ones and particularly their intensities, so that they seem to be first derivatives of peaks, but in fact they are related to the two different Raman processes.

d. The torsional potential energy surface and the energetic ordering of the 2-FPEA conformers

As a first step toward the identification of the measured ILSR spectra, the conformational preferences of the 2-FPEA molecule in its ground electronic state, S_0, were determined. These preferences were obtained by initiating the geometry optimization from one of the conformers of 2-FPEA and by performing a PES grid search at the MP2/6-311++G(d,p) level of theory. As mentioned above, the grid search for 2-FPEA was performed by scanning the ψ and β dihedral angles (Fig. 1) in steps of 10°.

The resulting PES of 2-FPEA and the structures of its conformers are shown in Fig. 6(a) and (b), respectively. Fig. 6(b) also includes the computed energies of the minima, in the phenyl ring of each structure, and of the transition states (first-order saddle points), near the arrows marking the direction of the transition from a conformer to the other, as determined from the torsional PES.

The PES is characterized by nine unique minima, six of them related to *gauche* conformers with the amino group pointing toward the fluorine atom (G1f, G2f and G3f) or to the opposite side (G1h, G2h and G3h), and three related to *anti* conformers with an extended ethylamino side chain (A1h, A2 and A1f). It can be seen from Fig. 6 that the highest energy barriers are between the two types of *gauche* conformers, and the energy barrier is somewhat lower between the *gauche* and *anti* conformers. Even lower barriers are observed between the different conformers in each column.

In particular, the global minimum is related to the G1h *gauche* conformer [Fig. 6(b)], and the two additional *gauche* conformers, G2h and G2f, where the NH_2 group possesses different orientations, are somewhat higher in energy and separated from each other, and from the global minimum, by relatively high potential barriers. These conformers are reached by varying the ψ and β dihedral angles (relative to those of G1h) for the former and latter, respectively. The following two additional minima, A1h and A2, result from *anti* conformers, which are separated by lower barriers from each other, and by

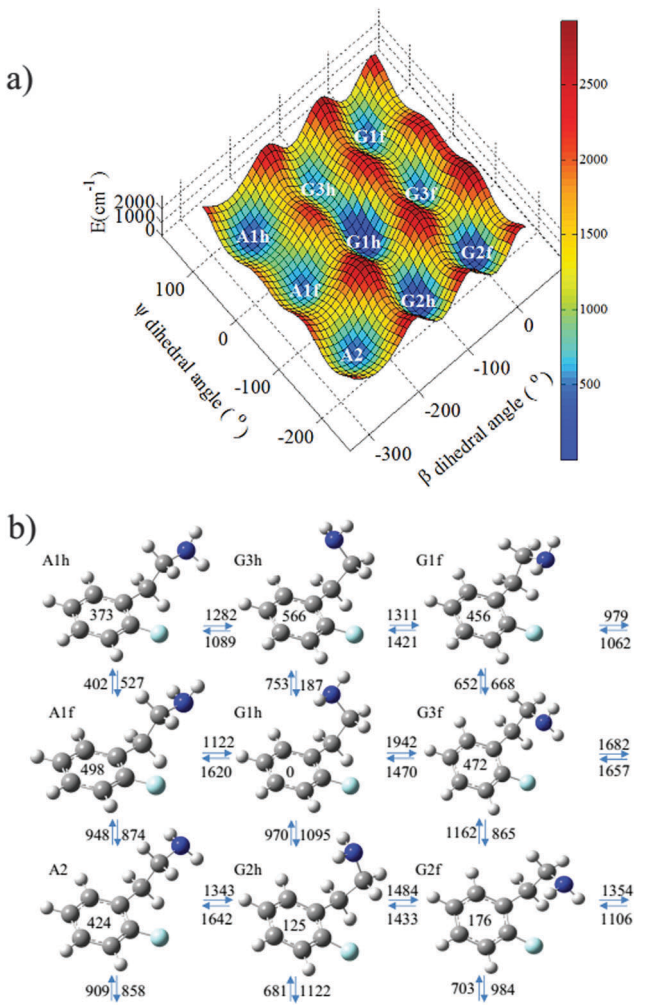

Fig. 6 (a) The potential energy surface (PES) of 2-(2-fluoro-phenyl)-ethylamine (2-FPEA) as a function of the ψ and β dihedral angles (Fig. 1) and (b) the structures of the nine energetically most favorable conformers of the 2-FPEA monomer, fully geometrically optimized in their ground electronic state, S_0. The computed energies (cm^{-1}) [MP2/6-311++G(d,p)] of the minima and of the transition states (first-order saddle points) as determined from the torsional PES are given in the phenyl rings of each structure and near the arrows pointing to the direction of the transitions, respectively.

higher barriers, along the β dihedral angles, that separate them from the *gauche* conformers. The additional conformers are even higher in energy and actually were not observed in our experiment and in the microwave study.[22]

These values of the global minima are also summarized in Table 2 and compared to the results computed at other levels of theory. The relative energies in Table 2 differ from those in Fig. 6(b), due to the fact that the former are true minima, while the latter are from the 10° grid. Actually, the ordering of the energies of the five most stable conformers (G1h, G2h, G2f, A1h, A2) is similar to that for the values obtained at the MP2/6-311++G(d,p) level of theory with corrections for zero-point vibrational energies from M06-2X/6-311++G(d,p) and B3LYP/6-311++G(d,p). This ordering also agrees with that obtained by Melandri *et al.*[22] at the MP2/6-311++G(d,p) level of theory. As for the higher energy conformers (G1f, G3f, A1f, G3h) the ordering obtained by the three methods does not exactly match. The ordering of these conformers depends on the calculation method and probably differs due to the very small changes in energy between them. It is anticipated that the M06-2X functional performs better than the B3LYP functional in terms of predicting the general trends in the relative energies of the conformers, since the dispersion interactions, taken into account by the former, contribute to the conformer energetics of 2-FPEA.

e. Identification of the conformers of 2-FPEA

As mentioned above, the assignment of the conformers of 2-FPEA is supported by evidence coming from calculations of structures and energetic ordering and especially by ILSR spectroscopy. It is obvious that the interpretation of the measured ILSR spectra and the identification of the conformers of 2-FPEA require high accuracy calculated Raman spectra. Eventually, by considering which are the most stable five conformers of 2-FPEA and by comparing the measured and calculated spectra we found the best matching ones and as a result revealed the conformers existing in the molecular beam. First attempts verified the resemblance of the measured ILSR spectra and Raman spectra calculated at the B3LYP/6-311++G(d,p) level of theory. However, since the patterns shown by the latter did not fit very well the measured spectra, difficulties were encountered in assigning the involved conformers. Consequently, dispersion-corrected M06-2X/6-311++G(d,p) Raman spectra were calculated and used for the comparison.

For instance, Fig. 7 shows the measured low frequency range ILSR spectrum of one of the conformers, G2h, of 2-FPEA [panel (a)] and the scaled harmonic Raman spectra, obtained by using the functionals M06-2X [panel (b)] and B3LYP [panel (c)], both with the 6-311++G(d,p) basis set. It can be seen, particularly for the features marked by the dashed lines, that their positions in the spectrum calculated at the M06-2X/6-311++G(d,p) level show smaller deviations from those observed in the experimental spectrum and generally reproduce it better. This behavior was also encountered for the other conformers, leading us to rely on the M06-2X/6-311++G(d,p) level of theory for finding the correspondence between the ILSR spectra and the specific structures of 2-FPEA.

Accordingly, the measured ILSR spectra of the different conformers of 2-FPEA, top traces of Fig. 4(a)–(e) and 5(a)–(e), were compared to the scaled harmonic Raman spectra [M06-2X/6-311++G(d,p)], shown in the bottom traces. As can be seen, the calculated spectra match relatively well the measured ILSR spectra, when different scaling factors were used for the low frequency range and for the various groups of vibrations in the high frequency range. In the low frequency range, where the vibrational signatures involve bending modes of the amino and the alkyl groups, as well as collective motions of most atoms in the molecule, the calculated spectra nicely mimic the patterns exhibited by the measured ILSR spectra. The measured spectra in Fig. 4(a)–(e) and 5(a)–(e) were consequently attributed to the G2h, G1h, A1h, G2f and A2 conformers of 2-FPEA, respectively.

Essentially, the high frequency range spectra include features corresponding to the N–H stretches of the ethylamino side chain and to C–H stretches of the ring and of the alkyl group. While the C–H stretches of the ring appear as four peaks

Table 2 Calculated relative energies, ΔE, and zero-point corrected energies, ΔE_0, of 2-(2-fluoro-phenyl)-ethylamine and of 2-phenylethylamine, in cm^{-1}, following M06-2X and B3LYP optimizations with subsequent MP2 single point energy calculations. All calculations were performed with the 6-311++G(d,p) basis set

	2-FPEA							PEA				
	M06-2X		B3LYP		MP2			M06-2X		B3LYP		MP2
	MP2	ZPE	MP2	ZPE	MP2	ZPE		MP2	ZPE	MP2	ZPE	ZPE
	ΔE	ΔE_0[a]	ΔE	ΔE_0[b]	ΔE[c]	ΔE_0[c]		ΔE[a]	ΔE_0[a]	ΔE[b]	ΔE_0[b]	ΔE_0[d]
G1h	0	0	0	0	0	0	G(I)	0	0	0	0	0
G2h	136	129	135	114	108	115	G(II)	121	86	120	105	128
G2f	183	190	164	149	162	199						
A1h	374	344	309	259	368	267	A(I)	472	392	409	349	382
A2	429	381	367	307	420	369	A(II)	498	416	434	372	406
G1f	462	430	473	435	452	383						
G3f	465	450	458	400	459	445						
A1f	493	451	429	364	487	379						
G3h	586	519	562	489	581	421						

[a] Zero-point corrections based on the M06-2X/6-311++G(d,p) level of theory. [b] Zero-point corrections based on the B3LYP/6-311++G(d,p) level of theory. [c] Values obtained at the MP2/6-311++G(d,p) level of theory, taken from Melandri *et al.*[22] [d] Values obtained at the MP2/6-311++G(d,p) level of theory, taken from López *et al.*[16a]

in the 3040–3080 cm^{-1} range in all five conformers, the N–H (3340–3460 cm^{-1}) and the C–H stretches (2870–2980 cm^{-1}) of the ethylamino group show some slight changes in frequencies and in patterns. Comparison of these changes in the antisymmetric (higher frequency and weaker feature) and symmetric (lower frequency and stronger feature) N–H stretches, respectively, while passing from one conformer to the next, shows a tendency of red and blue shifts, which is mimicked by the calculated spectra of the above mentioned 2-FPEA structures. In addition, the intensities of the measured peaks correspond nicely to the calculated ones. Explicitly, the *gauche* conformers of 2-FPEA show that the N–H symmetric stretches in the ILSR spectra are somewhat shifted to lower frequencies (G1h, G2h and G2f at 3346, 3345 and 3347 cm^{-1}, respectively) compared to the corresponding features of the *anti* conformers (A1h and A2 at 3350 and 3349 cm^{-1}, respectively). These small red displacements of the N–H symmetric stretch mode may indicate that in the *gauche* conformers, with the amino side chain folded toward the phenyl ring, the electron density is pulled away from the N–H bonds, with very minor changes from one conformer to the next. Accordingly, the interaction between a hydrogen atom of the amino group (on the folded side chain) and the electron cloud of the ring in 2-FPEA leads to weak N–H$\cdots\pi$ hydrogen bonds in the *gauche* conformers. It is interesting to note that the red shifts for the N–H symmetric stretches of the *gauche* conformers of 2-FPEA resemble those observed in the unsubstituted PEA. This implies that the strength of the N–H$\cdots\pi$ hydrogen bonds in the *gauche* conformers of both molecules is quite similar, although it may possibly be expected that the electron-withdrawing effect of the fluorine atom in 2-FPEA would lead to somewhat weaker interaction.

As for the alkyl C–H stretches, observation of four transitions related to the symmetric and antisymmetric stretch modes of the two different CH_2 groups would be anticipated. Indeed, in some of the spectra the number of resolved transitions is four, while in others some of the bands split up, probably due to Fermi resonances that couple the C–H stretches with overtones and combination bands of the CH_2 bends. Yet, it is apparent from the spectra that the alkyl C–H stretch region is sensitive to the conformation of the ethylamino side chain in 2-FPEA. It can be seen that the spectra in panels (b) and (c) of Fig. 5 exhibit features that are characterized by a triplet separated from the lowest Raman shifted line, while the other spectra include two pairs of lines that differ in spacing between them. The calculated Raman spectra in the C–H stretch region for conformers G1h (the most stable one) and A1h of 2-FPEA, panels (b) and (c) of Fig. 5, respectively, correlate well with the experimental ILSR spectra and indicate that the symmetric C–H stretch on C8 shifts to <2880 cm^{-1}. As for the other conformers, no quantitative fit between the measured ILSR and calculated Raman spectra is observed. This could be a result of the scaled harmonic frequency calculations that were performed, which fail to reach the required accuracy in the computed C–H stretch force field and also do not account for the Fermi resonances, anharmonic couplings and local mode mixing, and therefore do not provide the exact values for the C–H stretch frequencies. These findings show that the C–H stretches in the ILSR spectra are very sensitive to the amino group orientation and are probably influenced by the interaction of the CH_2 moiety with the lone pair electrons on nitrogen.

Nevertheless, the assignment of the 2-FPEA conformers is greatly assisted by the low frequency range spectra (Fig. 4). It is immediately apparent that for all conformers the dominant measured ILSR features, and even most of the low intensity ones, are well reproduced by the calculated Raman spectra. Comparison of the spectra, related to the different conformers, shows that some of the features appear at almost identical frequencies, while others exhibit shifts, due to changes in the structure. A region that shows very different patterns in the ILSR spectra of the 2-FPEA conformers is that around 1000 cm^{-1}, Fig. 4, displayed as an expanded portion in Fig. 8. Also shown on the right of each panel in Fig. 8 are the geometries of the respective conformers together with the displacement vectors, generated by Gaussview.[41] These vectors graphically represent a pair of normal modes of the two highest frequency vibrations, related to collective motions of the atoms in the different conformers. In fact, only small changes appear in the frequency of the vibrational mode around 1040 cm^{-1}, which is attributed to the breathing mode of the ring, and therefore expected to be relatively insensitive to the structure of the different conformers. As for the other vibration, consisting of out-of-plane movement of the C–H groups of the ring and of the alkyl moieties of the tail, the shifts to lower frequencies are as much as 65 cm^{-1}, depending on the specific conformer.

Consequently, the good agreement between the measured ILSR and computed Raman spectra provides evidence that the structures of 2-FPEA, on which the scaled harmonic frequency calculations are based, may be reliable, enabling us to assign the structures of the conformers existing in the cold molecular

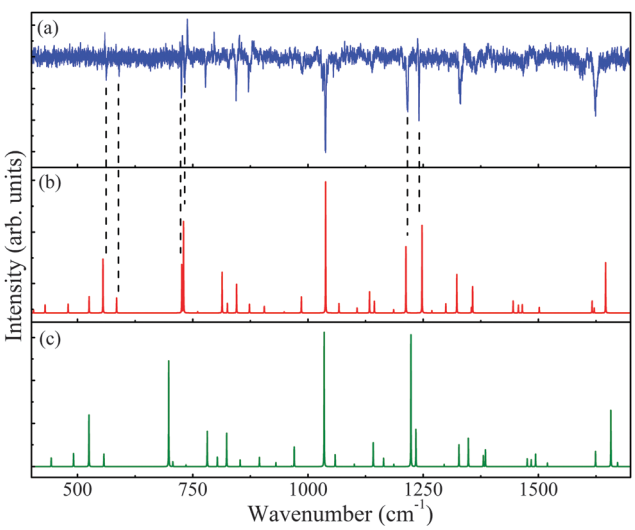

Fig. 7 Comparison of the (a) measured ionization-loss stimulated Raman spectrum of the G2h conformer of 2-(2-fluoro-phenyl)-ethylamine with the calculated Raman spectrum at the (b) M06-2X/6-311++G(d,p) and (c) B3LYP/6-311++G(d,p) levels of theory.

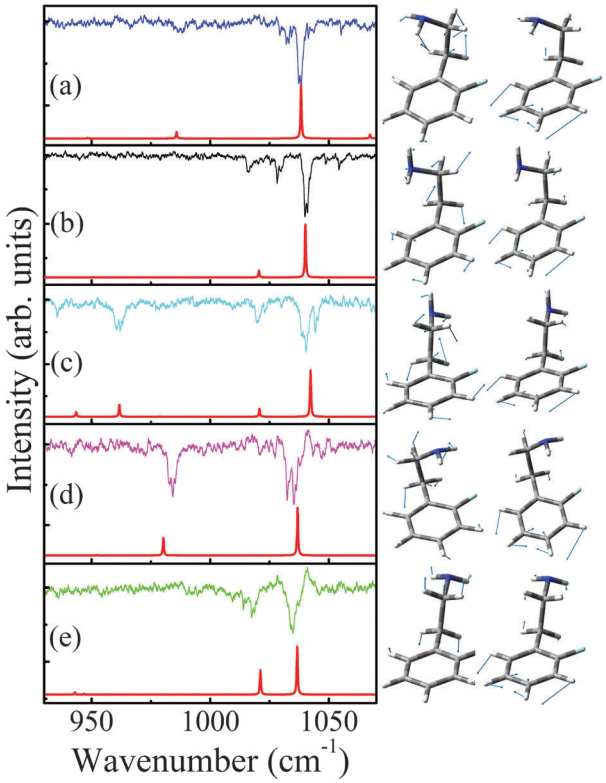

Fig. 8 Expanded portion of the ionization-loss stimulated Raman spectra of the conformers of 2-(2-fluoro-phenyl)-ethylamine, G2h (a), G1h (b), A1h (c), G2f (d) and A2 (e), in the 1000 cm^{-1} region. Below each experimental spectrum a calculated one, exhibiting the closest agreement, is shown. On the right of each panel, the geometries of the respective conformers together with the displacement vectors corresponding to the normal modes of the two highest frequency vibrations are shown.

beam. The observation of five different spectra for the conformers of 2-FPEA and their comparison with the calculated spectra confirmed that the low and high frequency features, shown in Fig. 4(a)–(e) and 5(a) and (e), correspond to the G2h, G1h, A1h, G2f and A2 conformers of 2-FPEA, respectively, also identified in the microwave study.[22]

This interpretation is also supported by the energetic ordering predicted by the quantum chemical calculations shown in Fig. 6 and in Table 2. As mentioned above, the G1h conformer of 2-FPEA corresponds to the global minimum and the *gauche* conformers, G2h and G2f, and the *anti* conformers, A1h and A2, are somewhat higher in energy. The relatively high potential energy barriers between these conformers render them experimentally distinguishable. As for the four additional computed conformers, G1f, G3f, A1f and G3h, they are even higher in energy, but exhibit lower potential barriers for isomerization, implying that they would not persist in the molecular beam.

The fluorination in 2-FPEA, with the fluorine atom in the *ortho* position, introduces an asymmetry in the molecule and exerts a delicate stabilizing effect that increases the number of conformers, when compared to the non-fluorinated analog PEA. This explains our observation of five discernible conformers in the former, instead of four in the latter,[10,16a,18a] as reflected by the somewhat smaller gaps in energy between the most stable structures of 2-FPEA (Table 2). Actually, as can be seen from the data in Table S2 of the ESI,† the action of the bonding interactions, between the hydrogen of the amino group and the center of the π system, N–H···F, C–H···F, and that between the nitrogen carrying the lone pair electrons and the hydrogen atom, N(lp)···H, as well as the repulsive interaction between the nitrogen and fluorine, N(lp)···F(lp), span over a large range of values. This implies that these bonding and repulsive interactions play a major role in establishing the stable structures of the various conformers of 2-FPEA, being determined by the available number of interactions as well as by their strength.

It is very satisfying to find out that the same five conformers were found in the molecular beams of three setups, while using very different methods based on microwave spectroscopy,[22] UV–UV HB and ILSRS, where the last two methods confirm the previous findings of the former. These are the first measurements of the vibrational and electronic spectra of the 2-FPEA conformers, where the former allowed, through comparison with theoretical calculations, one to distinguish between numerous conformational structures. This work is of importance due to the methodological demonstration of the use of ILSRS both in the N–H stretch region and in the broad spectral range, where the former allowed finding the different conformers that exist in the molecular beam and the latter obtaining the structures of the congested conformers of 2-FPEA. The assignment of the conformers was assisted by the access of low- and high-frequency regions, which provided information on the collective as well as on the localized vibrational motions, respectively. It is anticipated that the ILSR spectra in the extended range would allow one to distinguish between conformational structures, even in cases in which the more widespread infrared double-resonance techniques do not lead to unequivocal assignments. The intramolecular interactions stabilizing the conformational structures of this neurotransmitter analog have only been slightly considered in the microwave study[22] as well as in this work and certainly deserve further characterization in the future.

4. Conclusions

As can be inferred from the above, this study shows the premise behind our approach, where vibrational spectra were measured by the ILSR method in a broad spectral range, enabling us to monitor multiple vibrational modes of the different conformers of 2-FPEA. The ILSR and UV–UV HB spectra confirmed the existence of five different conformers of 2-FPEA in the molecular beam. The interpretation and identification of the available conformers of 2-FPEA in the molecular beam became possible by the comparison of the experimental ILSR spectra with the computed Raman spectra. The good correlation between the measured ILSR spectra and the calculated ones allowed us to find out that *gauche* conformers, including G1h, as the global minimum, and the G2h and G2f conformers, as well as the *anti* conformers, A1h and A2, persist in the

molecular beam. These results also bring support to the fact that the harmonic Raman spectra, calculated by the dispersion-corrected M06-2X/6-311++G(d,p) level of theory, reproduce better the experimental ILSR spectra and mimic better the observed patterns than spectra calculated at the B3LYP/6-311++G(d,p) level.

The substitution of a specific hydrogen atom with the fluorine atom in the *ortho* position produces an asymmetric structure for 2-FPEA with the fluorine being in close proximity to the ethylamino side chain, slightly modifying the energetic ordering and the energy gaps between the various conformers. This energetic arrangement derives from the interplay between the hydrogen bonds and the repulsive interactions, which exert a delicate stabilizing effect that increases the number of conformers, when compared to the non-fluorinated analog PEA. It would be of interest to examine the effect of fluorine substitution in the *para*-position, where the symmetry of PEA is kept, on the conformational landscape.

Acknowledgements

We thank Sonia Melandri (University of Bologna) for fruitful discussions. Financial support of this research by the German-Israeli Foundation for Scientific Research and Development (G.I.F.) under Grant no. 1164-158.5/2011, the Israel Science Foundation (ISF) founded by The Israel Academy of Sciences and Humanities, and the Deutsche Forschungsgemeinschaft (DO 729/4) is gratefully acknowledged.

References

1 E. G. Robertson and J. P. Simons, *Phys. Chem. Chem. Phys.*, 2001, **3**, 1–18.
2 T. S. Zwier, *J. Phys. Chem. A*, 2001, **105**, 8827–8839.
3 M. S. de Vries and P. Hobza, *Annu. Rev. Phys. Chem.*, 2007, **58**, 585–612.
4 M. Mons, I. Dimicoli and F. Piuzzi, *Int. Rev. Phys. Chem.*, 2002, **21**, 101–135.
5 J. M. Berg, J. L. Tymoczko and L. Stryer, *Biochemistry*, W. H. Freeman, New York, 6th edn, 2006.
6 H. Mitsuda, M. Miyazaki, I. B. Nielsen, P. Çarçabal, C. Dedonder, C. Jouvet, S. Ishiuchi and M. Fujii, *J. Phys. Chem. Lett.*, 2010, **1**, 1130–1133.
7 S. J. Martinez III, J. C. Alfano and D. H. Levy, *J. Mol. Spectrosc.*, 1993, **158**, 82–92.
8 P. D. Godfrey, L. D. Hatherley and R. D. Brown, *J. Am. Chem. Soc.*, 1995, **117**, 8204–8210.
9 (*a*) S. Sun and E. R. Bernstein, *J. Am. Chem. Soc.*, 1996, **118**, 5086–5095; (*b*) J. Yao, H. S. Im, M. Foltin and E. R. Bernstein, *J. Phys. Chem. A*, 2000, **104**, 6197–6211.
10 (*a*) J. A. Dickinson, M. R. Hockridge, R. T. Kroemer, E. G. Robertson, J. P. Simons, J. McCombie and M. Walker, *J. Am. Chem. Soc.*, 1998, **120**, 2622–2632; (*b*) M. R. Hockridge and E. G. Robertson, *J. Phys. Chem. A*, 1999, **103**, 3618–3628.
11 R. Weinkauf, F. Lehrer, E. W. Schlag and A. Metsala, *Faraday Discuss.*, 2000, **115**, 363–381.
12 (*a*) J. R. Carney and T. S. Zwier, *J. Phys. Chem. A*, 2000, **104**, 8677–8688; (*b*) B. C. Dian, A. Longarte and T. S. Zwier, *J. Chem. Phys.*, 2003, **118**, 2696–2706; (*c*) J. R. Clarkson, B. C. Dian, L. Moriggi, A. DeFusco, V. McCarthy, K. D. Jordan and T. S. Zwier, *J. Chem. Phys.*, 2005, **122**, 214311.
13 W. Caminati, *Phys. Chem. Chem. Phys.*, 2004, **6**, 2806–2809.
14 M. Schmitt, M. Böhm, C. Ratzer, C. Vu, I. Kalkman and W. L. Meerts, *J. Am. Chem. Soc.*, 2005, **127**, 10356–10364.
15 T. Nguyen and D. W. Pratt, *J. Chem. Phys.*, 2006, **124**, 054317.
16 (*a*) J. C. López, V. Cortijo, S. Blanco and J. L. Alonso, *Phys. Chem. Chem. Phys.*, 2007, **9**, 4521–4527; (*b*) C. Cabezas, I. Peña, J. C. López and J. L. Alonso, *J. Phys. Chem. Lett.*, 2013, **4**, 486–490.
17 M. Böhm, R. Brause, C. Jacoby and M. Schmitt, *J. Phys. Chem. A*, 2009, **113**, 448–455.
18 (*a*) A. Golan, N. Mayorkas, S. Rosenwaks and I. Bar, *J. Chem. Phys.*, 2009, **131**, 024305; (*b*) N. Mayorkas, I. Malka and I. Bar, *Phys. Chem. Chem. Phys.*, 2011, **13**, 6808–6815; (*c*) N. Mayorkas, S. Izbitski, A. Bernat and I. Bar, *J. Phys. Chem. Lett.*, 2012, **3**, 603–607; (*d*) N. Mayorkas, A. Bernat, S. Izbitski and I. Bar, *J. Chem. Phys.*, 2013, **138**, 124312.
19 S. Melandri, A. Maris, B. M. Giuliano, L. B. Favero and W. Caminati, *Phys. Chem. Chem. Phys.*, 2010, **12**, 10210–10214.
20 I. A. Lobo, D. J. D. Wilson, E. Bieske and E. G. Robertson, *Phys. Chem. Chem. Phys.*, 2012, **14**, 9219–9229.
21 R. Karaminkov, S. Chervenkov and H. J. Neusser, *Phys. Chem. Chem. Phys.*, 2008, **10**, 2852–2859.
22 S. Melandri, A. Merloni and A. Maris, *ChemPhysChem*, 2012, **13**, 3504–3509.
23 (*a*) N. A. Macleod and J. P. Simons, *Phys. Chem. Chem. Phys.*, 2003, **5**, 1123–1129; (*b*) N. A. Macleod and J. P. Simons, *Mol. Phys.*, 2006, **104**, 3317–3328.
24 (*a*) A. Lagutschenkov, J. Langer, G. Berden, J. Oomens and O. Dopfer, *J. Phys. Chem. A*, 2010, **114**, 13268–13276; (*b*) A. Lagutschenkov, J. Langer, G. Berden, J. Oomens and O. Dopfer, *Phys. Chem. Chem. Phys.*, 2011, **13**, 2815–2823; (*c*) A. Lagutschenkov, J. Langer, G. Berden, J. Oomens and O. Dopfer, *Phys. Chem. Chem. Phys.*, 2011, **13**, 15644–15656; (*d*) A. Bouchet, M. Schütz, B. Chiavarino, M. E. Crestoni, S. Fornarini and O. Dopfer, *Phys. Chem. Chem. Phys.*, 2015, **17**, 25742–25754; (*e*) B. Chiavarino, M. E. Crestoni, M. Schütz, A. Bouchet, S. Piccirillo, V. Steinmetz, O. Dopfer and S. Fornarini, *J. Phys. Chem. A*, 2014, **118**, 7130–7138; (*f*) A. Bouchet, M. Schütz and O. Dopfer, *ChemPhysChem*, DOI: 10.1002/cphc.201500939.
25 (*a*) J. R. Clarkson, J. M. Herbert and T. S. Zwier, *J. Chem. Phys.*, 2007, **126**, 134306; (*b*) T. A. LeGreve, W. H. James III and T. S. Zwier, *J. Phys. Chem. A*, 2009, **113**, 399–410.
26 N. Mayorkas, S. Cohen, H. Sachs and I. Bar, *RSC Adv.*, 2014, **4**, 58752–58757.
27 J. Wang, M. Sánchez-Roselló, J. L. Aceña, C. del Pozo, A. E. Sorochinsky, S. Fustero, V. A. Soloshonok and H. Liu, *Chem. Rev.*, 2014, **114**, 2432–2506.
28 D. Cantacuzene, K. L. Kirk, D. H. McCulloh and C. R. Creveling, *Science*, 1979, **204**, 1217–1219.
29 B. K. Park, N. R. Kitterngham and P. M. O'Neill, *Annu. Rev. Pharmacol. Toxicol.*, 2001, **41**, 443–470.

30 K. Müller, C. Faeh and F. Diederich, *Science*, 2007, **317**, 1881–1886.
31 G. V. Hartland, B. F. Henson, V. A. Venturo, R. A. Hertz and P. M. Felker, *J. Opt. Soc. Am. B*, 1990, **7**, 1950–1959.
32 M. Epshtein, A. Portnov, R. Kupfer, S. Rosenwaks and I. Bar, *J. Chem. Phys.*, 2013, **139**, 184201.
33 S. Ishiuchi, T. Asakawa, H. Mitsuda, M. Miyazaki, S. Chakraborty and M. Fujii, *J. Phys. Chem. A*, 2011, **115**, 10363–10369.
34 Avogadro: an open-source molecular builder and visualization tool, Version 1.00, http://avogadro.openmolecules.net/; M. D. Hanwell, D. E. Curtis, D. C. Lonie, T. Vandermeersch, E. Zurek and G. R. J. Hutchison, *J. Cheminf.*, 2012, **4**, 17.
35 M. J. Frisch, G. W. Trucks, H. B. Schlegel, G. E. Scuseria, M. A. Robb, J. R. Cheeseman, G. Scalmani, V. Barone, B. Mennucci, G. A. Petersson, H. Nakatsuji, M. Caricato, X. Li, H. P. Hratchian, A. F. Izmaylov, J. Bloino, G. Zheng, J. L. Sonnenberg, M. Hada, M. Ehara, K. Toyota, R. Fukuda, J. Hasegawa, M. Ishida, T. Nakajima, Y. Honda, O. Kitao, H. Nakai, T. Vreven, J. A. Montgomery Jr, J. E. Peralta, F. Ogliaro, M. Bearpark, J. J. Heyd, E. Brothers, K. N. Kudin, V. N. Staroverov, R. Kobayashi, J. Normand, K. Raghavachari, A. Rendell, J. C. Burant, S. S. Iyengar, J. Tomasi, M. Cossi, N. Rega, J. M. Millam, M. Klene, J. E. Knox, J. B. Cross, V. Bakken, C. Adamo, J. Jaramillo, R. Gomperts, R. E. Stratmann, O. Yazyev, A. J. Austin, R. Cammi, C. Pomelli, J. W. Ochterski, R. L. Martin, K. Morokuma, V. G. Zakrzewski, G. A. Voth, P. Salvador, J. J. Dannenberg, S. Dapprich, A. D. Daniels, Ö. Farkas, J. B. Foresman, J. V. Ortiz, J. Cioslowski and D. J. Fox, *Gaussian 09, revision C.01*, Gaussian, Inc., Wallingford, CT, 2009.
36 A. D. Becke, *Phys. Rev. A: At., Mol., Opt. Phys.*, 1988, **38**, 3098–3100.
37 C. Lee, W. Yang and R. G. Parr, *Phys. Rev. B: Condens. Matter Mater. Phys.*, 1988, **37**, 785–789.
38 Y. Zhao and D. G. Truhlar, *Theor. Chem. Acc.*, 2008, **120**, 215–241.
39 C. Møller and M. S. Plesset, *Phys. Rev.*, 1934, **46**, 618–622.
40 T. Kim and P. M. Felker, *J. Phys. Chem. A*, 2007, **111**, 12466–12470.
41 R. Dennington II, T. Keith and J. Millam, *et al.*, *Gaussview, Version 3.09*, Semichem Inc., Shawnee Mission, KS, 2003.